Talnakhite: a potential n-type thermoelectric sulphide with low thermal conductivity

Mukherjee, S., Powell, A. V., Voneshen, D. J. and Vaqueiro, P. ORCID: https://orcid.org/0000-0001-7545-6262 (2022)
Talnakhite: a potential n-type thermoelectric sulphide with low thermal conductivity. Journal of Solid State Chemistry, 314. 123425. ISSN 0022-4596 doi: 10.1016/j.jssc.2022.123425
Available at https://centaur.reading.ac.uk/106163/

Journal of Solid State Chemistry 314 (2022) 123425

Contents lists available at ScienceDirect

Journal of Solid State Chemistry

journal homepage: www.elsevier.com/locate/jssc

Talnakhite: A potential *n*-type thermoelectric sulphide with low thermal conductivity

Shriparna Mukherjee [a], Anthony V. Powell [a,**], David J. Voneshen [b,c], Paz Vaqueiro [a,*]

[a] Department of Chemistry, University of Reading, Whiteknights, Reading, RG6 6DX, United Kingdom
[b] ISIS Pulsed Neutron and Muon Source, Rutherford Appleton Laboratory, Chilton, Didcot, Oxon, OX11 0QX, United Kingdom
[c] Department of Physics, Royal Holloway University of London, Egham, TW20 0EX, United Kingdom

ARTICLE INFO

Keywords:
Sulphides
n-type
Thermoelectric material
Thermal conductivity
Substitution

ABSTRACT

The mineral talnakhite, $Cu_{18}Fe_{16}S_{32}$, is an *n*-type semiconductor with low thermal conductivity (average value of 1.5 W m^{-1} K^{-1}), making it an attractive candidate for thermoelectric applications. The effect of partial cation substitutions and of deviations from the ideal Cu:Fe ratio on the thermoelectric properties of this material, has been investigated through synthesis of $Cu_{17.58}M_{0.02}Fe_{17.6}S_{32}$ (M = Ag, In, Zn) and $Cu_{17.6+x}Fe_{17.6-x}S_{32}$ ($-0.03 \leq x \leq 0.03$) by high-temperature methods. The results demonstrate that talnakhite exhibits a narrow range of compositional stability for substitution at the cation sites. X-ray photoelectron spectroscopy (XPS) measurements indicate that all compositions contain Fe^{3+} and Fe^{2+} cations, together with Cu^{+}. The electrical and thermal transport properties show two anomalies, at approximately 460 and 510 K, which can be related to structural phase transitions. The maximum value of the thermoelectric figure of merit occurs at the temperature of the first structural phase transition, making talnakhite a potential *n*-type candidate for near room-temperature thermoelectric applications. While substitution with silver, zinc or indium does not lead to any significant improvement in thermoelectric performance, changes in the Cu:Fe ratio result in significant reductions in the total thermal conductivity. This is likely to be associated with increased point defect scattering due to the presence of additional vacancies at the cation sites over which iron and copper are partially ordered. For copper-poor phases, the combination of a slightly improved power factor with a reduced thermal conductivity results in an increase in the figure-of-merit by approximately 20% when compared to the stoichiometric phase.

1. Introduction

Growing concerns about sustainable energy sources have stimulated considerable research efforts into efficient and cost-effective thermoelectric (TE) devices, to enable the conversion of waste heat into electrical power [1–3]. To facilitate widespread adoption of TE energy recovery, the discovery of non-toxic, earth-abundant materials with good TE performance is essential. The efficiency of a TE material is related to a dimensionless figure-of-merit, $zT=(S^2\sigma T)/\kappa$, which is dependent on the Seebeck coefficient (S), electrical conductivity (σ) and thermal conductivity (κ) [3]. In order to achieve a high figure-of-merit, a material requires a high electrical conductivity, like that of a metal, combined with a large Seebeck coefficient and low thermal conductivity; properties normally associated with insulating materials. Construction of TE devices requires *p*- and *n*-type materials.

Recently, ternary and quaternary copper sulphide minerals have attracted much interest owing to their abundance, low cost and promising TE performance [4]. Several *p*-type sulphides with excellent TE performance have been identified following suitable doping, including bornite, Cu_5FeS_4 ($zT \sim 0.79$ at 550 K) [5], colusite, $Cu_{26}V_2Sn_6S_{32}$ ($zT \sim 0.9$ at 675 K) [6], and tetrahedrite, $Cu_{12}Sb_4S_{13}$ ($zT \sim 1$ at 720 K) [7]. However, there is a dearth of the *n*-type counterparts with comparable TE performance required for the construction of a TE device. Examples of *n*-type copper sulphides with moderate figures of merit include $CuFe_2S_3$ ($zT \sim 0.14$ at 700 K) [8], Cu_2ZnSnS_4 ($zT \sim 0.35$ at 700 K) [9], $Cu_4Sn_7S_{16}$ ($zT \sim 0.27$ at 700 K) [10] and $CuFeS_2$ ($zT \sim 0.21$ at 573 K) [11]. Of these, chalcopyrite ($CuFeS_2$), which is the most common copper-bearing mineral, is an attractive candidate, as it contains Earth-abundant elements only. However, the high thermal conductivity in chalcopyrite limits its TE performance [12–15].

* Corresponding author. Department of Chemistry, University of Reading, Reading, RG6 6DX, United Kingdom.
** Corresponding author.
E-mail addresses: a.v.powell@reading.ac.uk (A.V. Powell), p.vaqueiro@reading.ac.uk (P. Vaqueiro).

https://doi.org/10.1016/j.jssc.2022.123425
Received 25 May 2022; Received in revised form 5 July 2022; Accepted 10 July 2022
Available online 13 July 2022

In the region of the Cu–Fe–S phase diagram where chalcopyrite is located, a number of structurally-related phases exist, in which the elemental ratios deviate from the 1:1:2 stoichiometry of chalcopyrite. These phases include talnakhite, mooihoekite and haycockite [16,17]. Talnakhite ($Cu_{18}Fe_{16}S_{32}$) is a metal-rich mineral, with a structure closely related to that of chalcopyrite. While chalcopyrite adopts a zinc blende superstructure in which ordering of copper and iron atoms results in a doubling of the unit cell along the *c*-axis, talnakhite adopts a "stuffed" zinc blende superstructure (Fig. 1), in which the excess cations are accommodated in interstitial tetrahedral sites. This results in short metal-metal distances of *ca.* 2.7 Å, and hence the crystal structure of talnakhite contains octahedral metal clusters (Fig. 1 (b)), similar to those found in colusites [18] and tetrahedrites [19], two families of materials with remarkably low thermal conductivities. Bonding heterogeneity, such as the coexistence of covalent metal-sulphur bonds and metal-metal bonds, that is common to talnakhite, tetrahedrites and colusites, has been identified as a characteristic that can increase phonon scattering and therefore lower the lattice thermal conductivity [20,21]. Indeed, a recent study has shown that talnakhite is an *n*-type semiconductor which exhibits a low lattice thermal conductivity, of *ca.* 0.6 W m^{-1} K^{-1} at 625 K [22]. Despite this highly promising thermal conductivity, and in contrast to the extensive doping studies carried out on chalcopyrite [14,15,23–25], the optimization of the charge carrier density of talnakhite to maximize zT has not been explored.

In this work, we investigate the effect of a range of metal substituents on the thermoelectric properties of talnakhite. In order to reduce the thermal conductivity further, we have explored isovalent substitution of Cu^+ with larger Ag^+ cations, which for the closely related chalcopyrite, has led to a reduction in lattice thermal conductivity [26]. To increase the power factor, we have investigated aliovalent substitution of Cu^+ with trivalent In^{3+} and divalent Zn^{2+} in talnakhite, since for chalcopyrite those substituents have led to increases in charge carrier concentration [23,27]. Furthermore, we also sought to investigate adjustments to the Cu:Fe ratio in talnakhite, given the remarkable enhancements in the figure of merit (up to 44% increase) that have been achieved in bornite (Cu_5FeS_4) by adjusting both the Cu:Fe ratio and vacancy concentration [5].

2. Experimental details

Although the nominal composition of the mineral talnakhite has been reported as $Cu_{18}Fe_{16}S_{32}$ [28], a previous study indicates that synthesis of single-phase talnakhite requires a stoichiometry of $Cu_{17.6}Fe_{17.6}S_{32}$ [22]. This composition was therefore used for the work described here, with the materials with the nominal composition $Cu_{17.6}Fe_{17.6}S_{32}$ designated 'unsubstituted talnakhite'. Polycrystalline materials of composition $Cu_{17.6+x}Fe_{17.6-x}S_{32}$ ($-0.03 \leq x \leq 0.03$) and $Cu_{17.58}M_{0.02}Fe_{17.6}S_{32}$ (M = Ag, In, Zn) were prepared by solid-state synthesis. Elemental copper (99.5%), iron (99.9+%) and sulphur (99.99%) were sealed into evacuated ($<10^{-4}$ mbar) fused-silica ampoules. The sealed ampoules were heated to 573 K (at a rate of 0.5 K min^{-1}) and held for 6 h at this temperature. The temperature was then increased to 1173 K at the same rate, held for 48 h and reduced slowly to room temperature (at a rate of 0.1 K min^{-1}). The solid products were ground into a fine powder and consolidated into densified pellets by hot pressing at 823 K and 70 MPa for 30 min. The density of the hot-pressed pellets was determined by the Archimedes' method, using an AE Adam PW 184 balance. All the pellets have a density greater than 96% of the crystallographic density of talnakhite.

Powder X-ray diffraction (XRD) patterns were collected using a Bruker D8 Advance Powder X-ray diffractometer, operating with Ge-monochromated Cu $K\alpha_1$ (λ = 1.54046 Å) radiation. Unit-cell parameters were determined by Le-Bail refinement, performed using the Fullprof package [29]. Energy dispersive spectrometry (EDS) analysis was carried out on a FEI Quanta FEG 600 ESEM, operating with a voltage of 20 kV in high vacuum mode. Heat flow (differential scanning calorimetry) data over the temperature range $300 \leq T/K \leq 575$ were collected under a flowing N_2 atmosphere using a TA-Q2000 DSC instrument. X-ray Photoelectron Spectroscopy (XPS) data were acquired using a Kratos Axis Ultra DLD using monochromatic Al K_α (1486.69 eV) radiation and an analysis area of *ca.* 700 × 300 μm. Spectra were charge corrected to the main line of the carbon 1*s* spectrum (adventitious carbon) set to 284.8 eV. All data were recorded at a pressure below 1×10^{-9} Torr and at a temperature of 294 K. XPS data were analyzed using CasaXPS v2.3.24 [30], with the elemental sensitivity factors as supplied by the manufacturer. Peaks were defined using a Shirley background prior to component analysis.

Thermoelectric properties were measured over the temperature range $300 \leq T/K \leq 575$. The electrical conductivity and Seebeck coefficient were measured simultaneously using a LINSEIS LSR 3 instrument under a helium atmosphere. A current of 20 mA was used for the conductivity measurements and a gradient of 50 K was maintained between the upper and lower electrodes for measurement of the Seebeck coefficient. Graphite-coated circular pellets with a diameter of 12.7 mm and thickness ~1.5–2 mm were used for the thermal diffusivity (D) measurements using a NETZSCH LFA 447 NanoFlash system. Data were analyzed using Cowan's model with a pulse correction applied. The thermal conductivity (κ) was then calculated from the relation, $\kappa = DdC_p$ where d is the density of the material and C_p is the specific heat capacity. Here, the Dulong Petit limit for C_p (example, C_p for $Cu_{17.6}Fe_{17.6}S_{32}$ = 0.535 J g^{-1} K^{-1}) has been

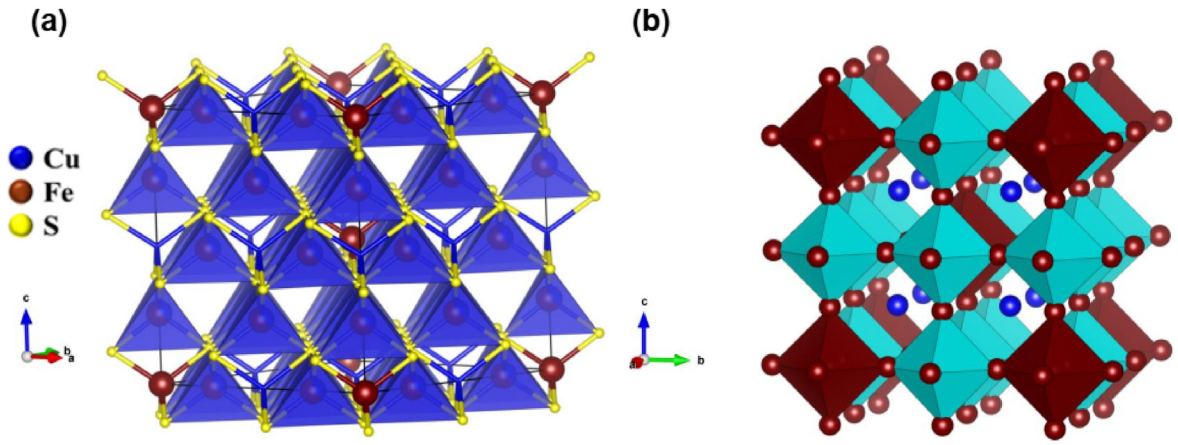

Fig. 1. (a) Crystal structure of talnakhite $Cu_{18}Fe_{16}S_{32}$. Blue spheres represent Cu atoms, brown spheres represent Fe atoms and yellow spheres represent S atoms. (b) The three-dimensional network of cation-centered octahedra arising from metal-metal bonding (sulphur atoms omitted for clarity). Pastel blue octahedra represent Cu/vacancy-centered octahedra; brown octahedra represent iron-centered octahedra.

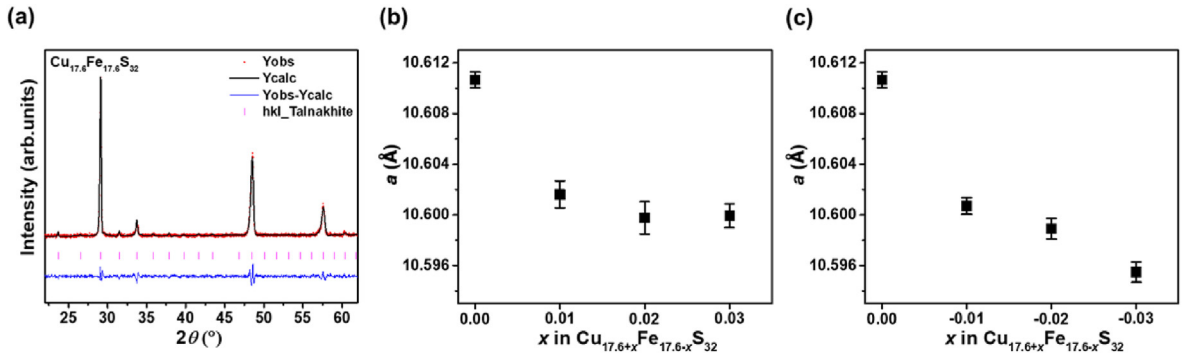

Fig. 2. (a) Powder X-ray diffraction pattern for unsubstituted talnakhite ($Cu_{17.6}Fe_{17.6}S_{32}$), together with analysis by the structure-independent Le Bail method. Comparison of lattice parameters between unsubstituted talnakhite ($x = 0$) (b) copper-rich and (c) copper-poor series.

used in the calculations. The electronic part of the thermal conductivity (κ_e) was calculated using the Wiedemann-Franz law ($\kappa_e = L\sigma T$ where L is the Lorenz number) and the lattice thermal conductivity κ_l as the difference ($\kappa - \kappa_e$). The Lorenz number (L) was obtained assuming a single parabolic band approximation (SPB) and numerically solving a set of equations involving the Seebeck coefficients (obtained from the transport measurements) and the reduced chemical potential [3] (details are provided in the Supplementary Material). The carrier concentration of the materials was measured using an ECOPIA HMS-3000 Hall effect measurement system. A magnetic field of 0.56 T and currents between 1 and 10 mA were used for the Hall measurements. The effective mass of carriers (m^*) was calculated following the Mott formula $S = \frac{8\pi^2 k_B^2}{3eh^2} m^* T \left(\frac{\pi}{3n}\right)^{2/3}$.

3. Results and discussion

3.1. Structural characterization and phase behaviour

Powder X-ray diffraction data (PXRD) for all materials reported here reveal the formation of a cubic phase (Fig. 2(a) and Supplementary Material Fig. S1), which can be indexed in the space group $I\bar{4}3m$ adopted by talnakhite [16]. Lattice parameters determined using Le Bail refinements (Fig. 2(b and c) and Supplementary Material Table S1) are in good agreement with those of talnakhite [22]. Substitution with indium and silver results in the formation of small amounts of chalcopyrite, while no additional peaks are found in the powder diffraction pattern of the Zn-substituted sample. For $Cu_{17.6+x}Fe_{17.6-x}S_{32}$ ($-0.03 \leq x \leq 0.03$), single-phase behaviour is retained for $-0.02 \leq x \leq 0.01$. At higher levels of substitution ($x > 0.01$ and $x < -0.02$), trace amounts of a tetragonal chalcopyrite-type phase can be observed in the diffraction data. Unit-cell parameters of the substituted phases are slightly reduced (< 0.5%) from those of the ternary $Cu_{17.6}Fe_{17.6}S_{32}$ phase, while variations in the Cu:Fe ratio have a similar effect (Fig. 2(b) and (c), Supplementary Material Table S1).

The overall compositions of all prepared materials (Supplementary Material Table S2), determined using energy dispersive spectrometry (EDS), are in agreement with the respective nominal compositions. Due

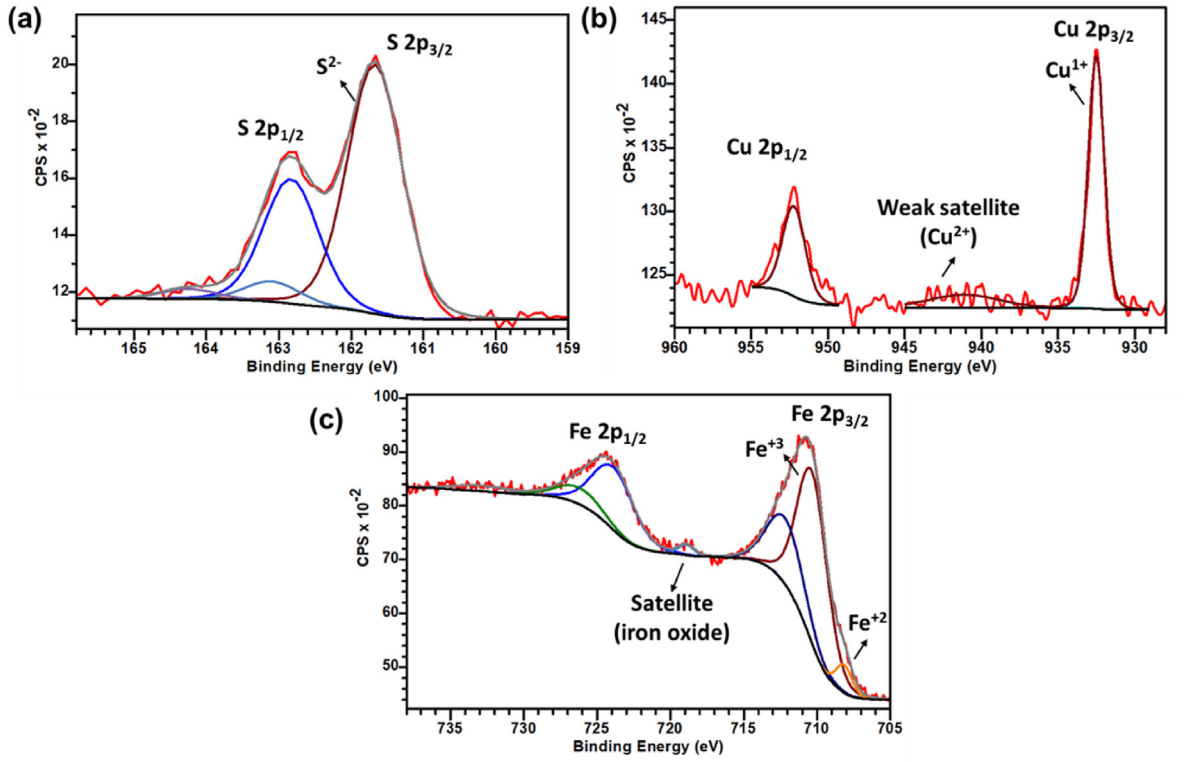

Fig. 3. X-ray photoelectron spectra for unsubstituted talnakhite showing (a) S $2p_{3/2}$ and $2p_{1/2}$, (b) Cu $2p_{3/2}$ and $2p_{1/2}$, and (c) Fe $2p_{3/2}$ and $2p_{1/2}$ core states.

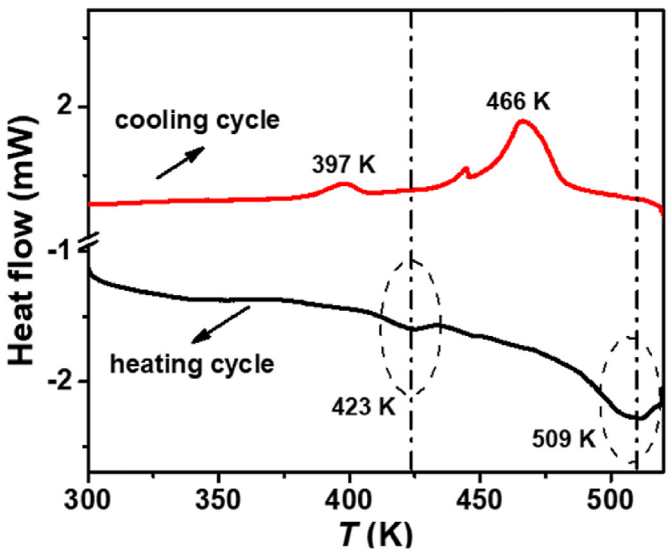

Fig. 4. DSC data for $Cu_{17.6}Fe_{17.6}S_{32}$. Vertical lines indicate the temperatures of the phase transitions in unsubstituted talnakhite.

to the lack of atomic number contrast, the chalcopyrite trace impurity is not apparent in the EDS maps measured on hot-pressed pellets for different compositions (Supplementary Material, Figure S2, S3 and S4). However, these maps indicate that the metal substituents are uniformly distributed throughout the ingots. SEM images for pellets with different compositions (Supplementary Material, Figs. S5 and S6) suggest that there are no significant changes in morphology with composition.

XPS measurements (Fig. 3) result in binding energies for S $2p_{3/2}$ and $2p_{1/2}$ at 161.6 eV and 162.8 eV respectively, typical for the sulphide S^{2-} anion [31]. A weak feature, centered at 168.7 eV and which can be attributed to S^{6+}, is found in some of the samples. This is likely to be the result of oxidation of the surface, to form SO_4^{2-}. The binding energies for Cu $2p_{3/2}$ and $2p_{1/2}$ peaks are centered at 932.5 eV and 952.4 eV respectively, indicating that Cu is primarily in the Cu^+ state [31,32]. In some samples, a very weak shake-up satellite peak, centered at 941.2 eV, can be assigned to the presence of trace amounts of Cu^{2+} [33]. The presence of this peak, together with the weak feature corresponding to S^{6+} may indicate that oxidation of the surface results in the formation of $CuSO_4$.

Analysis of the XPS data for the iron cations in talnakhite (Fig. 3 (c)) reveals that the Fe $2p_{3/2}$ peak is centered at 711.1 eV and the corresponding $2p_{1/2}$ peak is centered at 724.2 eV. These values are consistent with the presence of Fe^{3+}. A very weak satellite peak located at 718.8 eV has a binding energy comparable to those previously observed in XPS studies of iron oxides [34]. Moreover, the agreement between the calculated and observed XPS spectra improves upon introducing a component centered at 708.2 eV into the analysis. This suggests that Fe exists in both +3 and + 2 oxidation states, consistent with charge balancing requirements of the nominal composition of talnakhite, $(Cu^+)_{18}(Fe^{3+})_{14}(Fe^{2+})_2(S^{2-})_{32}$. Mössbauer spectra collected on talnakhite are also consistent with the presence of mixed-valent iron cations; the change in the isomer shifts of *ca.* 60% of the iron ions towards higher values when compared to those of Fe^{3+} in chalcopyrite are indicative of a lower average oxidation state [22]. In copper-rich materials, $Cu_{17.6+x}Fe_{17.6-x}S_{32}$ ($0.01 \leq x \leq 0.03$), the Cu to Fe ratio increases, hence the nominal Fe^{3+} content must also increase while Fe^{2+} content decreases. In copper-poor materials, $Cu_{17.6+x}Fe_{17.6-x}S_{32}$ ($-0.03 \leq x \leq -0.01$) the opposite occurs. Although XPS data confirm that both Fe^{3+} and Fe^{2+} are present in all compositions investigated, the variation in the relative Fe^{3+}: Fe^{2+} ratio expected on the basis of the nominal compositions is small, and hence the ratio cannot be determined reliably by XPS.

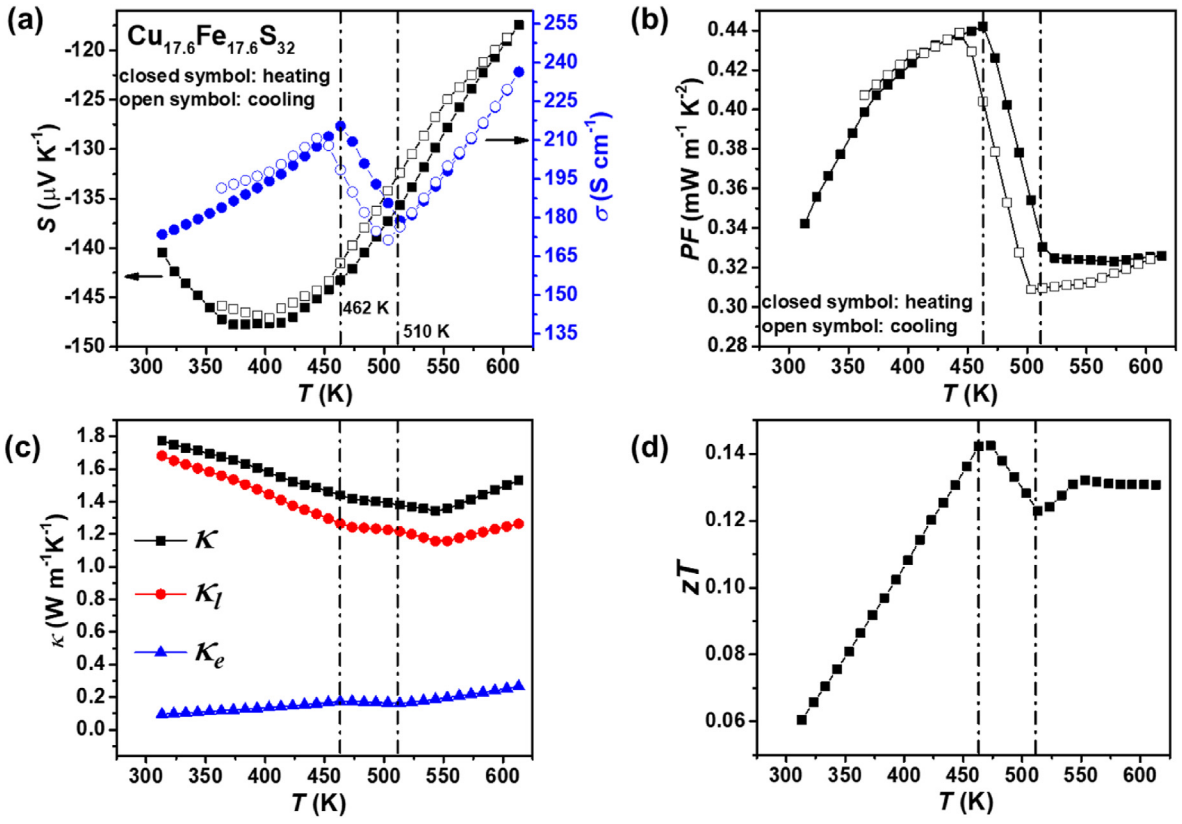

Fig. 5. Temperature dependence of the thermoelectric properties of $Cu_{17.6}Fe_{17.6}S_{32}$: (a) Electrical conductivity (σ) and Seebeck coefficient (S), (b) power factor, (c) thermal conductivity, and (d) figure-of-merit. Black vertical lines indicate the temperatures of the phase transitions in $Cu_{17.6}Fe_{17.6}S_{32}$.

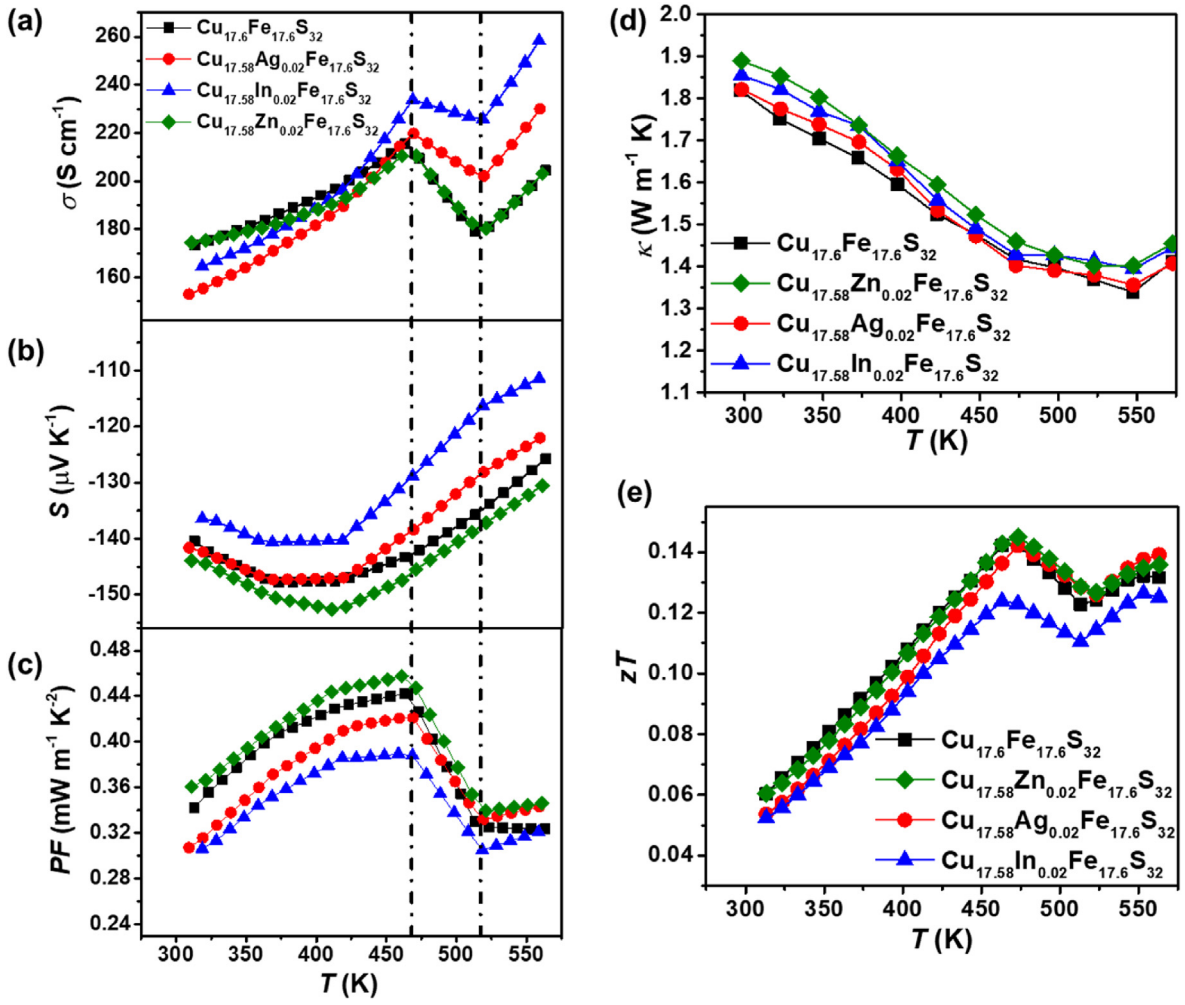

Fig. 6. The temperature dependent (a) electrical conductivity (σ), (b) Seebeck coefficient (S), (c) power factor (PF), (d) thermal conductivity (κ) and (e) figure of merit (zT) of $Cu_{17.58}M_{0.02}Fe_{17.6}S_{32}$ (where M = Zn, Ag, In). Black vertical lines indicate the temperatures of the phase transitions in talnakhite.

Previous studies indicate that talnakhite undergoes phase transitions at 460 and 503 K, before transforming into a sphalerite-like phase at 793 K [17]. However, the crystal structures of the phases present above room temperature have not been determined [17]. DSC data collected on unsubstituted talnakhite (Fig. 4) shows two endothermic peaks at *ca.* 423 K and 509 K on heating, with hysteresis occurring on cooling. While the peak at 509 K can be attributed to the second phase transition reported by Cabri [17], there is a significant difference between the temperature (423 K) of the first transition in the DSC data presented here, and those previously reported (460 K) by Cabri, on the basis of Guinier X-ray powder diffraction data [17]. An electron microscopy study by Putnis [16] indicates that the formation of partially-ordered and fully-ordered phases of talnakhite is governed by the kinetics of the processes involved. Given the different heating rates between the DSC and the X-ray diffraction measurements, this may be the origin of the discrepancy between the transition temperatures determined by DSC and by X-ray diffraction. Compositional changes are also likely to affect the temperature of the transition. A detailed structural study by powder X-ray and neutron diffraction is currently underway, to enable us to elucidate the origin of such transitions.

3.2. Thermoelectric properties

The thermoelectric properties of unsubstituted $Cu_{17.6}Fe_{17.6}S_{32}$ are presented in Fig. 5. The negative values of the Seebeck coefficient (S) (Fig. 5(a)), over the entire temperature range, indicate that electrons are the dominant charge carriers. The absolute value of the Seebeck coefficient reaches a maximum value of *ca.* 147 μV K^{-1} around 373–420 K. Thereafter, $|S|$ decreases, suggesting that this may correspond to the onset of bipolar conduction. The thermal band gap was estimated to be ~0.11 eV using the Goldsmid-Sharp relation, $E_g = 2e|S|_{max}T_{max}$ [35]. The band gap determined using this expression is not exact and significant deviations from the real band gap value can occur [35]. However, our attempts to determine the optical band gap by diffuse reflectance, over the wavelength range $200 \leq \lambda/nm \leq 2500$, were unsuccessful, indicating that the optical absorption edge of talnakhite occurs below 0.5 eV. This is broadly consistent with the estimated band gap of 0.11 eV.

Table 1
Hall Carrier concentration (n), Hall mobility (μ) and effective mass (m^*) of the materials measured at room temperature.

Nominal Composition	n (× 10^{19} cm^{-3})	μ (cm^2 V^{-1} s^{-1})	Effective mass (m^*/m_0)
$Cu_{17.6}Fe_{17.6}S_{32}$	5.8(1)	16.3(2)	1.29
$Cu_{17.58}Zn_{0.02}Fe_{17.6}S_{32}$	6.2(1)	15.0(2)	1.38
$Cu_{17.58}In_{0.02}Fe_{17.6}S_{32}$	4.9(1)	15.3(2)	1.11
$Cu_{17.58}Ag_{0.02}Fe_{17.6}S_{32}$	4.0(1)	14.8(2)	1.01
$Cu_{17.61}Fe_{17.59}S_{32}$	5.4(1)	18.4(2)	1.22
$Cu_{17.62}Fe_{17.58}S_{32}$	4.25(2)	19.5(5)	1.01
$Cu_{17.63}Fe_{17.57}S_{32}$	4.15(1)	17.6(2)	1.00
$Cu_{17.59}Fe_{17.61}S_{32}$	4.7(2)	15.9(6)	1.12
$Cu_{17.58}Fe_{17.62}S_{32}$	5.80(2)	14.1(1)	1.14
$Cu_{17.57}Fe_{17.63}S_{32}$	6.2(2)	16.1(1)	1.40

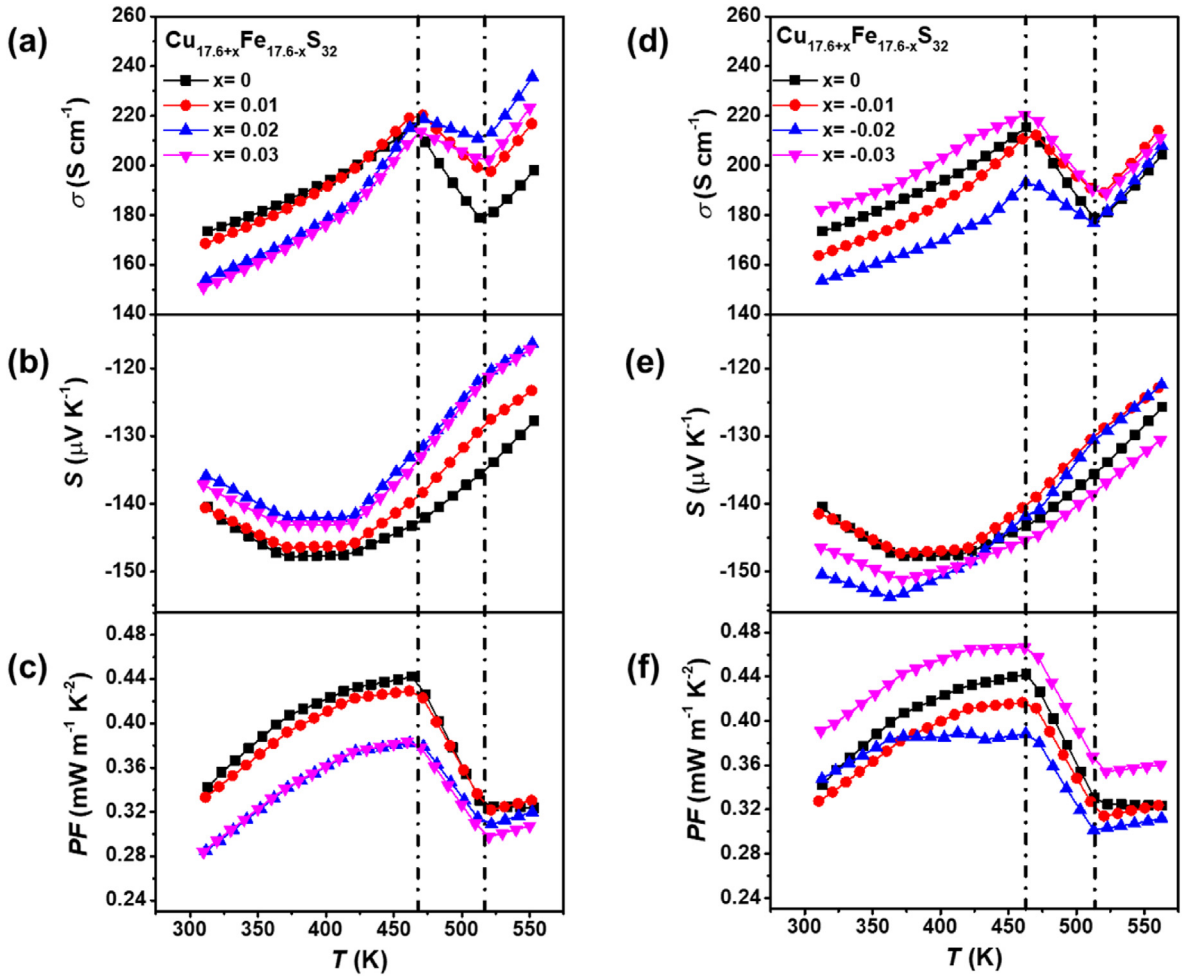

Fig. 7. (a) Electrical conductivity (σ), (b) Seebeck coefficient (S) and (c) power factor (PF) as a function of temperature for copper-rich $Cu_{17.6+x}Fe_{17.6-x}S_{32}$ (where $0 \leq x \leq 0.03$). (d) Electrical conductivity (σ), (e) Seebeck coefficient (S) and (f) power factor (PF) as a function of temperature for copper-poor $Cu_{17.6+x}Fe_{17.6-x}S_{32}$ (where $-0.03 \leq x \leq 0$). Black vertical lines indicate the temperatures of the phase transitions in talnakhite.

The electrical conductivity (σ) of unsubstituted $Cu_{17.6}Fe_{17.6}S_{32}$ increases with increasing temperature, as would be expected for a non-degenerate semiconductor, but shows two anomalies at 460 and 510 K, which correspond to the temperatures of the two phase transitions, according to a Guinier X-ray powder diffraction study of talnakhite [17]. The hysteresis observed between the heating and cooling cycles (Fig. 5(a)) is likely to be associated with the phase transitions. The highest power factor ($S^2\sigma$) (Fig. 5(b)) of 0.44 mW m^{-1} K^{-2} is obtained at 460 K, the temperature at which the first phase transition occurs.

As illustrated in Fig. 5(c), the principal contribution to the total thermal conductivity is the lattice term (κ_l). It should be noted that the total thermal conductivity of unsubstituted talnakhite prepared using SPS at 873 K for 5 min [22] is 1.56 W m^{-1} K^{-1} at room temperature, which is lower than the value of 1.77 W m^{-1}K^{-1} obtained here for samples hot-pressed at 823 K for 30 min. This difference is more marked at higher temperatures, with the SPS sample reaching a value of *ca.* 1.0 W m^{-1} K^{-1} at 570 K. It has been previously found that, in the case of colusite ($Cu_{26}V_2Sn_6S_{32}$), the thermal conductivity varies markedly depending on the consolidation method and conditions [6]. This variation has been attributed to sulphur volatilization and the formation of disordered domains when higher temperatures are used for consolidation. Electron microscopy data collected on talnakhite consolidated by SPS indeed indicates the presence of Cu-rich and Fe-rich areas on the micro- and nanoscale [22], which are likely to reduce the thermal conductivity.

Unlike $CuFeS_2$ [14,15,23–25], talnakhite exhibits an intrinsically low thermal conductivity, with an average value of *ca.* 1.5 W m^{-1} K^{-1} (for hot-pressed samples), leading to a figure-of-merit (zT) of 0.14 at 460 K (Fig. 5(d)). The origin of such low thermal conductivity has been attributed to weaker metal-sulphur bonds which, according to phonon calculations, lead to anharmonicity and the presence of low-energy optical modes [22]. Moreover, disordering of copper and iron cations and cation vacancies also results in point defect scattering and mass fluctuation scattering.

The temperature dependence of S, σ, and κ in the metal-substituted phases ($Cu_{17.58}M_{0.02}Fe_{17.6}S_{32}$ where M = Zn, In and Ag) is similar to that of unsubstituted talnakhite, $Cu_{17.6}Fe_{17.6}S_{32}$ (Fig. 6). Aliovalent substitution of Cu^+ with Zn^{2+} increases the Seebeck coefficient throughout the measured temperature range, whereas substitution with In^{3+} reduces the Seebeck coefficient. Moreover, the electrical conductivity is unchanged upon Zn-substitution, while In-substitution lowers the electrical conductivity at temperatures below the first phase transition.

Hall coefficient measurements (Table 1) indicate that Zn-substitution increases the Hall carrier concentration from that of the parent unsubstituted talnakhite phase, in agreement with formal charge considerations. Zn^{2+} is therefore an effective electron donor, as previously reported for chalcopyrite [23]. Both the Hall carrier concentration and electrical conductivity are reduced on indium substitution, which is contrary to expectations based on formal charge considerations. This could be the result of indium substituting at iron sites rather than at copper sites. In talnakhite, this would correspond to isovalent substitution of (mainly) Fe^{3+} by In^{3+}, accompanied by the introduction of

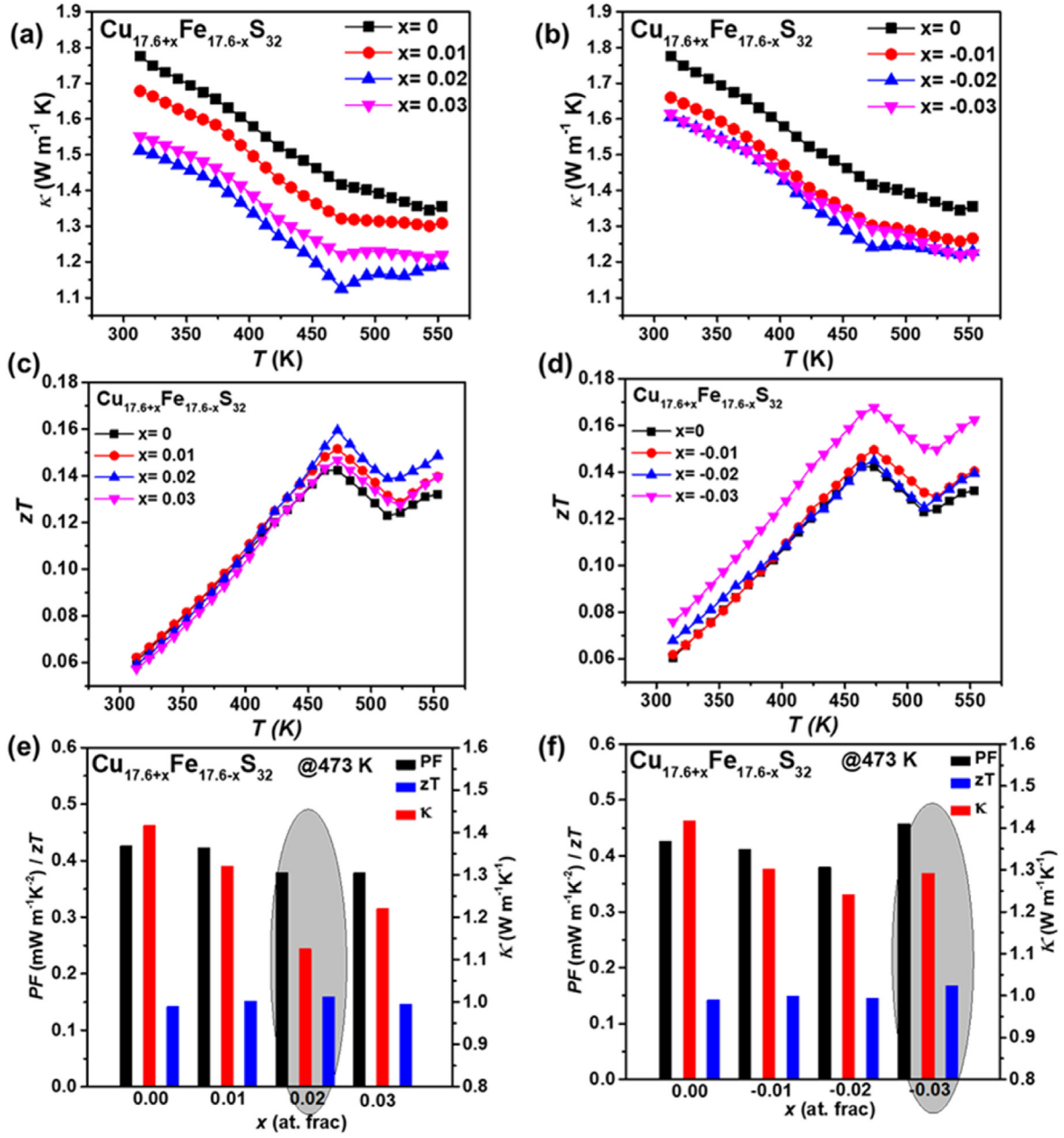

Fig. 8. (a) and (b) Temperature dependent thermal conductivity (κ) of copper rich ($0 \leq x \leq 0.03$) and copper poor ($-0.03 \leq x \leq 0$) talnakhites, respectively. (c) and (d) Temperature dependent figure of merit (zT) of copper rich ($0 \leq x \leq 0.03$) and copper poor ($-0.03 \leq x \leq 0$) talnakhites, respectively. Comparison of the figure of merit (zT), power factor (PF) and thermal conductivity (κ) for (e) copper-rich and (f) copper-poor talnakhites at 473 K. Values for the best performing materials are highlighted in grey.

vacancies at the copper sites, which would be consistent with the observed reduction in charge carrier concentration. Moreover, the presence of heavier In^{3+} will lead to alloy scattering of the charge carriers, and hence decrease their carrier mobility, in agreement with our experimental observations. In the case of chalcopyrite, substitution at both the copper and the iron sites has been explored, through preparation of $Cu_{1-x}In_xFeS_2$ [27] and $CuFe_{1-x}In_xS_2$ [36]. In the case of $Cu_{1-x}In_xFeS_2$, Xie et al. [27] have carried out DFT calculations to show that incorporation of In^+ is energetically favorable when compared with In^{3+} substitution at the Cu^+ site. As this would correspond to isovalent substitution of Cu^+ by In^+, the effect on the charge carrier concentration would be negligible. To the best of our knowledge, calculations to establish whether indium substitution is more favorable at the copper or at the iron sites have not been performed. Ionic radii [37] considerations would suggest that In^{3+} (0.62 Å) would replace Cu^+ (0.6 Å), rather than the smaller Fe^{3+} cation (0.49 Å), and that In^+, with an estimated ionic radius of 1.32 Å [38] would be too large. However, the electrical transport properties of $Cu_{17.58}In_{0.02}Fe_{17.61}S_{32}$ appear to be consistent with isovalent substitution of In^{3+} by Fe^{3+}, accompanied by the introduction of copper vacancies, rather than with aliovalent substitution of Cu^+ by In^{3+}.

Isovalent substitution of silver at the copper sites has little effect on the Seebeck coefficient at temperatures up to that of the first phase transition. Silver substitution reduces the carrier concentration (Table 1) and electrical conductivity in this temperature range. Similar results have been reported for $Cu_{1-x}Ag_xGaTe_2$ ($0 \leq x \leq 1$) [39] which, like $Cu_{17.58}Ag_{0.02}Fe_{17.6}S_{32}$, behaves as a non-degenerate semiconductor. The lower electrical conductivity for the Ag-substituted material may reflect increased scattering of charge carriers due to the presence of disordered Ag^+ cations, resulting in localised structural distortions, as they are larger

than the Cu^{+} cations they replace. This is consistent with the observed reduction in mobility (Table 1). The power factor shows little change from the parent talnakhite phase (Fig. 6 (c)).

Substitution of copper with heavier and larger cations would be expected to increase point defect scattering for phonons, due to mass and strain field fluctuations, and therefore reduce the lattice thermal conductivity. Surprisingly however, substitution with the heavier silver and indium cations has little impact on the thermal conductivity (Fig. 6(d)). Previous work on silver substitution in chalcopyrite suggests that reductions in thermal conductivity occur only at higher levels of substitution than reported here [26,39]. Unfortunately, this compositional region is inaccessible in talnakhite as secondary phases already present at the lower levels of substitution investigated here, become appreciable. Overall, there is no statistically significant improvement in the figure-of-merit on the introduction of metal substituents, as illustrated in Fig. 6 (e), with the introduction of indium leading to a slight reduction in zT.

Based on our previous work on the copper-iron sulphide, bornite (Cu_5FeS_4) [5], a different approach for tuning the thermoelectric properties was adopted, whereby the Cu:Fe ratio was varied through preparation of series of materials $Cu_{17.6+x}Fe_{17.6-x}S_{32}$ ($-0.03 \leq x \leq 0.03$). Since iron is likely to act as an electron donor, an increase in iron content can increase the electrical conductivity, as previously observed for iron-rich chalcopyrite [40].

As x increases, holes are doped into the system and the magnitude of the Seebeck coefficient decreases (Fig. 7 (a) and (b)) with a corresponding drop in the power factor (Fig. 7 (c)). The Hall carrier concentration (Table 1) also decreases in a systematic manner from 5.8×10^{19} cm^{-3} for $x = 0$ ($Cu_{17.6}Fe_{17.6}S_{32}$) to 4.15×10^{19} cm^{-3} for $x = 0.03$. The reduction in charge carrier concentration is accompanied by a small increase in Hall mobility (Table 1) in the Cu-rich talnakhites when compared to the unsubstituted phase. Higher mobility suggests a lower effective mass for the carriers resulting in lower Seebeck coefficients. Using the Mott formula, we found that the effective mass of the carriers decreases from 1.29 m_0 for $x = 0$ to 1.00 m_0 for $x = 0.03$. Therefore, the simultaneous decrease in electrical conductivity and Seebeck coefficient, which at first appears to be counterintuitive, is a consequence of a reduction in effective mass concomitant with the decrease in charge carrier concentration.

For the Cu-poor talnakhites, an increase in electron concentration is expected on substituting copper with iron. However, low levels of substitution result in a slight decrease in the charge carrier concentration (Table 1). Hence the electrical conductivity for materials corresponding to $x = -0.01$, -0.02 (Fig. 7 (d)–(f))) decreases when compared to that of the unsubstituted talnakhite. At higher levels of substitution ($x = -0.03$), both the electrical conductivity and the absolute value of the Seebeck coefficient increase from that of the parent phase, throughout the temperature range over which measurements were conducted. This results in a small improvement in the power factor, of *ca.* 5%, to 0.46 mW m^{-1} K^{-2} at 460 K for $x = -0.03$.

In marked contrast with the behavior on cation substitution, changes in the Cu:Fe ratio result in significant reductions in the total thermal conductivity: up to 20% in the Cu-rich series and up to 13% in the Cu-poor series (Fig. 8 (a) and (b)). For the composition with $x = 0.02$, the thermal conductivity approaches a minimum of *ca.* 1.12 W $m^{-1}K^{-1}$ at 473 K while for $x = -0.03$, $\kappa \approx 1.24$ W $m^{-1}K^{-1}$ at 473 K. This reduction in thermal conductivity may arise from an increase in point defect scattering due to the creation of vacancies. Although the total metal content in the series $Cu_{17.6+x}Fe_{17.6-x}S_{32}$ remains the same, in the complex crystal structure of talnakhite, iron and copper are partially ordered over five distinct crystallographic sites. The interstitial site 2*a* is occupied exclusively by iron, while the interstitial site 6*b*, which is partially occupied, contains only copper. Of the three cation sites forming the zinc blende superstructure (12*e*, 12*d* and 8*c*), 8*c* is occupied exclusively by copper, while 12*e* and 12*d* contain iron and copper [22,28]. Changes in x can create vacancies at sites that are preferentially occupied by iron (2*a*) or by copper (8*c* and 6*b*), resulting in a reduction in lattice thermal conductivity. Moreover, the secondary phases present at $x \geq 0.02$ and $x = -0.03$ can also act as additional phonon scattering centers, contributing to reducing the thermal conductivity. It is interesting to note that, although the electrical conductivity of the composition with $x = -0.03$ is increased over that of unsubstituted talnakhite, the total thermal conductivity for the substituted phase is lower. This is a consequence of a significant reduction (by 10%) in the lattice contribution for $x = -0.03$ when compared to that of unsubstituted talnakhite. The combination of an improved power factor and a lower thermal conductivity, results in a figure of merit for $Cu_{17.57}Fe_{17.63}S_{32}$ of $zT = 0.17$ at 473 K. This corresponds to an increase of *ca.* 20% over that of the parent phase ($zT \approx 0.14$) (Fig. 8 (c)–(f)).

4. Conclusions

The effect of a range of isovalent and aliovalent substituents, and of changes in the Cu:Fe ratio, on the phase behaviour and thermoelectric performance of talnakhite has been investigated. The talnakhite phase exhibits a narrow stability range, with impurities starting to appear at relatively low levels of substitution, up to $x \approx 0.02$. The electrical and thermal transport properties of all talnakhite-type phases investigated show two anomalies, at approximately 460 and 510 K, which may be attributed to two successive structural phase transitions. The thermoelectric power factor and the figure-of-merit of all samples reaches a maximum value at 460 K, the temperature at which the first phase transition occurs. This makes talnakhite a potential *n*-type candidate for near room-temperature thermoelectric applications. However, the narrow compositional range of the talnakhite structure, limits the capacity to increase the charge carrier concentration beyond *ca.* 6×10^{-19} cm^{-3} through substitution at the cation sites. The highest charge carrier concentration achieved in this study is two orders of magnitude lower than the optimal value of *ca.* 6–8 $\times 10^{21}$ cm^{-3} suggested by theoretical calculations for the closely-related $CuFeS_2$ [41]. Given the scarcity of *n*-type thermoelectric sulphides, and that talnakhite is a cost-efficient material with low thermal conductivity, further doping studies are required to achieve a significant increase in the charge carrier concentration. For the series $Cu_{17.6+x}Fe_{17.6-x}S_{32}$ ($-0.03 \leq x \leq 0.03$), changes in the Cu:Fe ratio led to significant reductions in the total thermal conductivity, of up to 20% in the Cu-rich series and up to 13% in the Cu-poor series, which arise as consequence of reductions in the lattice thermal conductivity. This reduction may be associated with increased point defect scattering due to the presence of additional vacancies at the cation sites over which iron and copper are partially ordered. Controlled introduction of vacancies at the cation sites, through preparation of materials in which the total metal content is varied from that of unsubstituted talnakhite, may facilitate further reductions in thermal conductivity.

Funding

The authors acknowledge The Leverhulme Trust for Research Project Grant RPG-2019-288.

CRediT authorship contribution statement

Shriparna Mukherjee: Conceptualization, Data curation, Formal analysis, Investigation, Writing – original draft. **Anthony V. Powell:** Funding acquisition, Writing – review & editing. **David J. Voneshen:** Funding acquisition, Writing – review & editing. **Paz Vaqueiro:** Conceptualization, Supervision, Funding acquisition, Project administration, Writing – original draft, Writing – review & editing.

Declaration of competing interest

The authors declare that they have no known competing financial interests or personal relationships that could have appeared to influence the work reported in this paper.

Data availability

Data will be made available on request.

Acknowledgements

The authors would like to thank the Chemical Analysis Facility at the University of Reading for access to powder X-ray diffraction, DSC and SEM instruments. X-ray photoelectron spectroscopy (XPS) data collection was performed at the EPSRC National Facility for XPS ("HarwellXPS"), operated by Cardiff University and UCL, under Contract No. PR16195.

Appendix A. Supplementary data

Supplementary data to this article can be found online at https://doi.org/10.1016/j.jssc.2022.123425.

References

[1] L.E. Bell, Cooling, heating, generating power, and recovering waste heat with thermoelectric systems, Science 321 (2008) 1457–1461.
[2] P. Ren, Y. Liu, J. He, T. Lv, J. Gao, G. Xu, Recent advances in inorganic material thermoelectrics, Inorg. Chem. Front. 5 (2018) 2380–2398.
[3] D.M. Rowe, C.M. Bhandari, Modern Thermoelectrics, Reston Publishing Company, INC., Reston, Virginia, 1983.
[4] A.V. Powell, Recent developments in Earth-abundant copper-sulfide thermoelectric materials, J. Appl. Phys. 126 (2019), 100901.
[5] S.O.J. Long, A.V. Powell, P. Vaqueiro, S. Hull, High thermoelectric performance of bornite through control of the Cu(II) content and vacancy concentration, Chem. Mater. 30 (2018) 456–464.
[6] C. Bourgès, Y. Bouyrie, A.R. Supka, R. Al Rahal Al Orabi, P. Lemoine, O.I. Lebedev, M. Ohta, K. Suekuni, V. Nassif, V. Hardy, R. Daou, Y. Miyazaki, M. Fornari, E. Guilmeau, High-performance thermoelectric bulk colusite by process controlled structural disordering, J. Am. Chem. Soc. 140 (2018) 2186–2195.
[7] X. Lu, D.T. Morelli, Y. Xia, F. Zhou, V. Ozolins, H. Chi, X. Zhou, High performance thermoelectricity in earth-abundant compounds based on natural mineral tetrahedrites, Adv. Energy Mater. (2013) 342–348.
[8] T. Barbier, D. Berthebaud, R. Frésard, O.I. Lebedev, E. Guilmeau, V. Eyert, A. Maignan, Structural and thermoelectric properties of n-type isocubanite $CuFe_2S_3$, Inorg. Chem. Front. 4 (2017) 424–432.
[9] M.L. Liu, F.Q. Huang, L.D. Chen, I.W. Chen, A wide-band-gap p -type thermoelectric material based on quaternary chalcogenides of Cu_2ZnSnQ_4 (Q=S,Se), Appl. Phys. Lett. 94 (2009) 46–49.
[10] T. Deng, T.R. Wei, Q. Song, Q. Xu, D. Ren, P. Qiu, X. Shi, L. Chen, Thermoelectric properties of n-type $Cu_4Sn_7S_{16}$-based compounds, RSC Adv. 9 (2019) 7826–7832.
[11] J. Li, Q. Tan, J.F. Li, Synthesis and property evaluation of $CuFeS_{2-x}$ as earth-abundant and and environmentally-friendly thermoelectric materials, J. Alloys Compd. 551 (2013) 143–149.
[12] N. Tsujii, T. Mori, High thermoelectric power factor in a carrier-doped magnetic semiconductor $CuFeS_2$, APEX 6 (2013), 043001.
[13] N. Tsujii, T. Mori, Y. Isoda, Phase stability and thermoelectric properties of $CuFeS_2$-based magnetic semiconductor, J. Electron. Mater. 43 (2014) 2371–2375.
[14] R. Lefèvre, D. Berthebaud, M.Y. Mychinko, O.I. Lebedev, T. Mori, F. Gascoin, A. Maignan, Thermoelectric properties of the chalcopyrite $Cu_{1-x}M_xFeS_{2-y}$ series (M = Mn, Co, Ni), RSC Adv. 6 (2016) 55117–55124.
[15] N. Tsujii, F. Meng, K. Tsuchiya, S. Maruyama, T. Mori, Effect of nanostructuring and high-pressure torsion process on thermal conductivity of carrier-doped chalcopyrite, J. Electron. Mater. 45 (2016) 1642–1647.
[16] A. Putnis, Talnakhite and Mooihoekite : the accessibility of ordered structures in the metal-rich region around chalcopyrite, Can. Mineral. 16 (1978) 23–30.
[17] L.J. Cabri, New data on phase relations in the Cu-Fe-S system, Econ. Geol. 68 (1973) 443–454.
[18] V. Pavan Kumar, G. Guélou, P. Lemoine, B. Raveau, A.R. Supka, R. Al Rahal Al Orabi, M. Fornari, K. Suekuni, E. Guilmeau, Copper-rich thermoelectric sulfides: size-mismatch effect and chemical disorder in the $[TS_4]Cu_6$ complexes of $Cu_{26}T_2Ge_6S_{32}$ (T=Cr, Mo, W) colusites, Angew. Chem. Int. Ed. 58 (2019) 15455–15463.
[19] S.O. Long, A.V. Powell, S. Hull, F. Orlandi, C.C. Tang, A.R. Supka, M. Fornari, P. Vaqueiro, Jahn–Teller driven electronic instability in thermoelectric tetrahedrite, Adv. Funct. Mater. 30 (2020), 1909409.
[20] M. Dutta, K. Pal, U.V. Waghmare, K. Biswas, Bonding heterogeneity and lone pair induced anharmonicity resulted in ultralow thermal conductivity and promising thermoelectric properties in n-type $AgPbBiSe_3$, Chem. Sci. 10 (2019) 4905–4913.
[21] N. Sato, N. Kuroda, S. Nakamura, Y. Katsura, I. Kanazawa, K. Kimura, T. Mori, Bonding heterogeneity in mixed-anion compounds realizes ultralow lattice thermal conductivity, J. Mater. Chem. A. 9 (2021) 22660–22669.
[22] H. Xie, X. Su, X. Zhang, S. Hao, T.P. Bailey, C.C. Stoumpos, A.P. Douvalis, X. Hu, C. Wolverton, V.P. Dravid, C. Uher, X. Tang, M.G. Kanatzidis, Origin of intrinsically low thermal conductivity in talnakhite $Cu_{17.6}Fe_{17.6}S_{32}$ thermoelectric material: correlations between lattice dynamics and thermal transport, J. Am. Chem. Soc. 141 (2019) 10905–10914.
[23] H. Xie, X. Su, G. Zheng, T. Zhu, K. Yin, Y. Yan, C. Uher, M.G. Kanatzidis, X. Tang, The role of Zn in chalcopyrite $CuFeS_2$: enhanced thermoelectric properties of Cu1–xZnxFeS2 with in situ nanoprecipitates, Adv. Energy Mater. 7 (2017), 1601299.
[24] D. Berthebaud, O.I. Lebedev, A. Maignan, Thermoelectric properties of n-type cobalt doped chalcopyrite $Cu_{1-x}Co_xFeS_2$ and p-type eskebornite $CuFeSe_2$, J. Mater. 1 (2015) 68–74.
[25] H. Xie, X. Su, G. Zheng, Y. Yan, W. Liu, H. Tang, M.G. Kanatzidis, C. Uher, X. Tang, Nonmagnetic in substituted $CuFe_{1-x}In_xS_2$ solid solution thermoelectric, J. Phys. Chem. C 120 (2016) 27895–27902.
[26] B. Ge, Z. Shi, C. Zhou, J. Hu, G. Liu, H. Xia, J. Xu, G. Qiao, Enhanced thermoelectric performance of N-type eco-friendly material $Cu_{1-x}Ag_xFeS_2$ (x=0–0.14) via bandgap tuning, J. Alloys Compd. 809 (2019), 151717.
[27] H. Xie, X. Su, S. Hao, C. Zhang, Z. Zhang, W. Liu, Y. Yan, C. Wolverton, X. Tang, M.G. Kanatzidis, Large thermal conductivity drops in the diamondoid lattice of $CuFeS_2$ by discordant atom doping, J. Am. Chem. Soc. 141 (2019) 18900–18909.
[28] S.R. Hall, Crystal structures of the chalcopyrite series, Can. Mineral. 13 (1975) 168–172.
[29] J. Rodriguez-Carvajal, Recent advances in magnetic structure determination by neutron powder diffraction + FullProf, Phys. B Condens. Matter 192 (1993) 55–69.
[30] N. Fairley, V. Fernandez, M. Richard-Plouet, C. Guillot-Deudon, J. Walton, E. Smith, D. Flahaut, M. Greiner, M. Biesinger, S. Tougaard, D. Morgan, J. Baltrusaitis, Systematic and collaborative approach to problem solving using X-ray photoelectron spectroscopy, Appl. Surf. Sci. Adv. 5 (2021), 100112.
[31] A. Ghahremaninezhad, D.G. Dixon, E. Asselin, Electrochemical and XPS analysis of chalcopyrite ($CuFeS_2$) dissolution in sulfuric acid solution, Electrochim. Acta 87 (2013) 97–112.
[32] D. Zhang, B. Zhang, Z.Z. Zhou, K. Peng, H. Wu, H. Wang, G. Wang, G. Han, G. Wang, X. Zhou, X. Lu, Ultralow lattice thermal conductivity of cubic $CuFeS_2$ induced by atomic disorder, Chem. Mater. 33 (2021) 9795–9802.
[33] M. Yin, C.K. Wu, Y. Lou, C. Burda, J.T. Koberstein, Y. Zhu, S. O'Brien, Copper oxide nanocrystals, J. Am. Chem. Soc. 127 (2005) 9506–9511.
[34] T. Yamashita, P. Hayes, Analysis of XPS spectra of Fe^{2+} and Fe^{3+} ions in oxide materials, Appl. Surf. Sci. 254 (2008) 2441–2449.
[35] Z.M. Gibbs, H. Kim, H. Wang, G.J. Snyder, Band gap estimation from temperature dependent Seebeck measurement — deviations from the 2e|S|max T max relation, Appl. Phys. Lett. 106 (2015), 022112.
[36] H. Xie, X. Su, G. Zheng, Y. Yan, W. Liu, H. Tang, M.G. Kanatzidis, C. Uher, X. Tang, Nonmagnetic in substituted $CuFe_{1-x}In_xS_2$ solid solution thermoelectric, J. Phys. Chem. C 120 (2016) 27895–27902.
[37] R.D. Shannon, Revised effective ionic radii and systematic studies of interatomic distances in halides and chalcogenides, Acta Crystallogaphica A32 (1976) 751–767.
[38] R.E. Jones, D.H. Templeton, The crystal structure of indium (I) iodide, Acta Crystallogaphica 8 (1955) 847.
[39] A. Yusufu, K. Kurosaki, Y. Ohishi, H. Muta, S. Yamanaka, Thermoelectric properties of chalcopyrite-type $CuGaTe_2$ with Ag substituted into the Cu sites, Jpn. J. Appl. Phys. 52 (2013).
[40] Y. Li, T. Zhang, Y. Qin, T. Day, G. Jeffrey Snyder, X. Shi, L. Chen, Thermoelectric transport properties of diamond-like $Cu_{1-x}Fe_{1+x}S_2$ tetrahedral compounds, J. Appl. Phys. 116 (2014), 203705.
[41] J. Park, Y. Xia, V. Ozoliņš, First-principles assessment of thermoelectric properties of $CuFeS_2$, J. Appl. Phys. 125 (2019), 125102.